
To fit or not to fit: Model-based Face Reconstruction and Occlusion Segmentation from Weak Supervision

Chunlu Li^{1,2} Andreas Morel-Forster² Thomas Vetter² Bernhard Egger^{3,*}
Adam Kortylewski^{4,*}

Abstract

3D face reconstruction from a single image is challenging due to its ill-posed nature. Model-based face autoencoders address this issue effectively by fitting a face model to the target image in a weakly supervised manner. However, in unconstrained environments occlusions distort the face reconstruction because the model often erroneously tries to adapt to occluded face regions. Supervised occlusion segmentation is a viable solution to avoid the fitting of occluded face regions, but it requires a large amount of annotated training data. In this work, we enable model-based face autoencoders to segment occluders accurately without requiring any additional supervision during training, and this separates regions where the model will be fitted from those where it will not be fitted. To achieve this, we extend face autoencoders with a segmentation network. The segmentation network decides which regions the model should adapt to by reaching balances in a trade-off between including pixels and adapting the model to them, and excluding pixels so that the model fitting is not negatively affected and reaches higher overall reconstruction accuracy on pixels showing the face. This leads to a synergistic effect, in which the occlusion segmentation guides the training of the face autoencoder to constrain the fitting in the non-occluded regions, while the improved fitting enables the segmentation model to better predict the occluded face regions. Qualitative and quantitative experiments on the CelebA-HQ database and the AR database verify the effectiveness of our model in improving 3D face reconstruction under occlusions and in enabling accurate occlusion segmentation from weak supervision only. Code available at <https://github.com/unibas-gravis/Occlusion-Robust-MoFA>.

1 Introduction

Monocular 3D face reconstruction aims at estimating the pose, shape, and albedo of a face, and the illumination conditions and camera parameters of the scene. Solving for all these factors from a single image is an ill-posed problem without additional assumptions. Model-based face autoencoders [27] tackle this issue by performing 3D reconstruction through fitting a 3D Morphable Model (3DMM) [1] to a target image. The 3DMM provides prior knowledge about the face appearance and geometry such that 3D face reconstruction from a single image becomes feasible. The network architectures in the face autoencoders are devised to enable end-to-end reconstruction and to enhance reconstruction speed compared to optimization-based alternatives [16, 33], and sophisticated losses are designed to stabilize the training and to get better performance [5].

¹ Dept. of Automation, Southeast University, Nanjing, 210096, China. (chunlu.li@unibas.ch)

² Dept. of Mathematics and Computer Science, University of Basel, Basel, CH 4051, Switzerland.

³ Dept. of Brain and Cognitive Sciences, Massachusetts Institute of Technology, Cambridge, MA 02215, USA.

⁴ Dept. of Computer Science, Johns Hopkins University, Maryland, MD 21218, USA.

* Denotes same contribution of Bernhard Egger (egger@mit.edu) and Adam Kortylewski (akortyl1@jhu.edu)



Figure 1: Our proposed method conducts face reconstruction and occlusion segmentation jointly, and is operated under weak supervision. From top to bottom: target images, our reconstruction images, and the estimated occlusion masks.

Despite the advances introduced by the face autoencoders, their performance on in-the-wild face reconstruction is still limited by nuisance factors such as occlusions, extreme illumination, and poses. Among those nuisances, occlusions are ubiquitous and inherently difficult to handle because of their wide variety in shape, appearance, and locations. A core problem caused by occlusion is that the face model adapts to occluded face regions and as a result, the 3D face reconstruction will be distorted.

Existing solutions to face reconstruction under occlusions often follow a bottom-up approach. For example, a multi-view shape consistency loss is used as prior to regularize the shape variation of the same face in different images [5, 9], and the face symmetry is used to detect occluders [29]. Most existing methods apply segmentation methods to locate the face region [25], or to detect skin [5] prior to the reconstruction, and subsequently exclude the occluded image regions during reconstruction. Most of these methods operate in a supervised manner and therefore demand significant efforts for acquiring a great variety of occlusions and annotations from in-the-wild images.

In this work, we enable model-based face autoencoders to locate occluded face regions during model training without requiring any additional supervision. This helps the network to distinguish the regions where the face model should adapt to from regions where the face model should not fit. The located occlusions are then excluded during training, so that only the unoccluded face regions can contribute to the gradient updates, and the occlusions do not affect the fitting adversely. To achieve this, we extend the face autoencoder architecture with a segmentation network that jointly predicts occluded face regions. To train the segmentation network, we exploit the generative nature of the face model. In particular, the output of the segmentation network is guided by the difference between the target image (Fig 1 first row) and the reconstructed image (Fig 1 second row). During training, the segmentation network balances a trade-off between including pixels and letting the model fit them, and excluding pixels so that the model is not negatively affected and reach higher overall reconstruction accuracy on pixels showing the face. This leads to a synergistic effect, in which the occlusion segmentation guides the training of the face autoencoder to constrain the fitting in the non-occluded face regions, while the improved fitting enables the segmentation model to better predict the occluded face regions.

The proposed model is trained end-to-end, following the core idea of the Expectation-Maximization (EM) algorithm, by alternating between training the face autoencoder given the predicted segmentation mask, and training the segmentation network based on the predicted 3D face reconstruction. The EM-like training strategy enables us to impose different losses on the two sub-networks, and it provides intervals for each network to adapt before the back-propagation changes the other network. Without the EM-like strategy, the segmentation results may change over time and consequently are not stable enough. In the whole training process, the only labels needed for supervision are the facial landmark positions, which guide the face autoencoder to estimate the face pose correctly. Unlike other methods which employ perceptual features for face reconstruction [5, 9] only, we propose to also take perceptual-level features into the loss when training the segmentation network to enable it to reason based on perceptual features. Generally, the perceptual features model small variations instead of stubborn comparing single pixels, therefore introducing these features renders the segmentation more robust to small variations in the face appearance. We use the perceptual-level features from a pretrained network [3] for face recognition, and refer to the loss as 'perceptual loss'.

We demonstrate the effectiveness of our method by conducting experiments on the CelebA-HQ dataset [17] and the AR database [19]. The experimental results show that our proposed pipeline reaches competitive fitting results and can provide faithful segmentation masks. Remarkably, our method is able to predict reliable occlusion masks without requiring any supervision during training.

In summary, we make the following contributions in this paper:

1. We introduce a new architecture for 3D face reconstruction that integrates model-based face autoencoders with an occlusion segmentation network and achieves largely enhanced occlusion robustness on in-the-wild images.
2. Our proposed architecture can be trained from weak supervision without requiring any manual occlusion annotation. This is achieved through the synergistic cooperation in which the occlusion segmentation guides the training of the face autoencoder to constrain the fitting in the non-occluded regions, while the improved fitting enables the segmentation model to better predict the occluded face regions.
3. The proposed architecture achieves competitive 3D face reconstruction on in-the-wild images and provides reliable estimates of the facial occlusion masks.

2 Related Work

Model-based face autoencoders [27] solve the 3D face reconstruction task by fitting a face model to the target image with an encoder and a renderer as the decoder. Typically, the encoder first estimates parameters from a target image, including the shape, texture, and pose of the target, and the illumination and camera settings from the scene. Then the renderer synthesizes a 2D image using the estimated parameters with an illumination model and a projection function. The face is reconstructed by retrieving the parameters which result in a synthesized image most similar to the target image. The 3DMM [1] plays a paramount role in the face autoencoders, because it parameterizes the latent distribution space of faces, and therefore can connect the encoder with the renderer and enable end-to-end training. The model-based face autoencoders have been proven effective in improving the reconstruction. They simplify the optimization step and enhance the reconstruction speed [28], improve the details of shape and texture [9, 10, 21, 29, 30], and can also reconstruct more discriminative features [5, 11].

Despite the advantages of the face autoencoders, their performance under occlusions is still limited. To solve this issue, some early methods [22] resort to robust fitting losses, but they are not robust to illumination variations and appearance variations in eye and mouth regions. In recent years, shape consistency losses have been used as prior to constrain the face shape across images of the same subject [5, 9, 26]. The variation of identity features of the 3D shape is restricted so that the shape reconstruction remains robust even in unconstrained environments. However, such methods usually need identity labels and do not promise robust texture reconstruction. Besides, many methods conduct face segmentation before reconstruction to lead the model to better fit the unoccluded face region. For example, a random forest detector for hair is proposed [20] so that the face model does not fit the hair region, and a semantic segmentation network is trained to better locate the face region [25]. A skin detector is employed to impose different weights on the pixels during reconstruction to guide the network to put more attention on the skin-colored regions and prevent it from fitting the occlusions [5]. However, the skin-colored occlusions, such as hair, hands, and so on, can not be distinguished correctly and the skin detector is sensitive to illumination. Yildirim et al. propose to explicitly model the 3D shape of certain types of occlusions and the shadow casted by them, in order to decompose the target into face regions and occlusions, and therefore the occlusions can be excluded during training [31]. However, the types of occlusions are limited. Similarly, attention masks are obtained in a supervised manner and are imposed on the intermediate layers of the encoder to suppress the influence of occlusions [24]. Generally, these off-the-shelf segmentation models require labeled data for training. Although using synthesized images can be used for training, there is a domain gap between the real images and the synthesized ones [15]. Unlike these methods, we merge the segmentation procedure into a model-based face autoencoder, which exploits the face model prior, and consequently does not require additional supervision.

The method which is most relevant to ours is proposed by Egger et al. [7]. They jointly adapt a face model to a target image and segment the target image into face, beard and occlusions. Their reconstruction and segmentation models are trained with an EM-like algorithm, where different



Figure 2: The architecture of the proposed pipeline. The solid arrows show the data flow in the model-based face autoencoder (blue) and the segmentation network (orange). The symbol \otimes indicates element-wise product.

models for beard, foreground, and background are optimized in alternating steps. Their method requires specific occlusion models and optimizes on each image separately in a non-learning manner instead of learning from a larger set of images. De Smet et al. also propose to conduct face model fitting and occlusion segmentation jointly [4], but they estimate the occlusions based on an appearance distribution model, which is sensitive to illumination variation and many other subtle changes in appearance. Maninchedda et al. propose to solve face reconstruction and segmentation in a joint manner [18], but depth maps are used to provide supervision. In comparison, our pipeline learns from only weak supervision and does not need specific models for different types of occlusions. The face autoencoder also enables us to adapt the face model more efficiently. In addition, we integrate perceptual losses which enable the segmentation network to reason over semantic features instead of making a decision based on independent pixels, to increase the robustness to illumination and other factors.

3 Approach

To handle occlusions for face reconstruction, we propose to conduct image segmentation and reconstruction jointly, so that the model-based face autoencoder and the segmentation network can supply information to each other and learn together. In the following, we illustrate the network architecture, the training strategy, and the initialization in detail.

3.1 Network Architecture

Given a target face image I_T , our goal is to jointly reconstruct the face and predict a binary mask M , for occlusion segmentation. To solve this problem, we propose to extend a model-based face autoencoder, R , with a segmentation network, S . The network architecture is demonstrated in Fig. 2.

The model-based face autoencoder, R , is expected to reconstruct the complete unoccluded face appearance from the visible face regions in the target image, I_T . It consists of an encoder and a renderer as its decoder. The encoder estimates the parameters of the 3D shape α , texture γ , and the pose p of the target, as well as the illumination ϕ and camera parameters c of the scene. These parameters are concatenated into one vector, $\theta = [\alpha, \gamma, p, \phi, c] \in \mathbb{R}^{257}$, as the latent representation of the face autoencoder. The shape and texture models are 3DMMs, and we refer to the survey [8] for more details. Then, the decoder renders a realistic intact image $I_R = R(I_T)$ of the target face based on the estimated parameters. We refer to the region where the rendered face spans as the **rendered region**, Φ . This procedure can be formulated as $R := I_T \mapsto \theta \mapsto I_R$, as illustrated in Fig. 2.

Without any specialized strategy handling occlusions, the autoencoder will fit the face model regardless of whether the underlying pixels depict face or occlusions. Consequently, the face model overfits the occluded regions. As shown in the first two rows in Fig. 3, the face encoder tends to darken the eye regions when there are sunglasses and alter the texture when the hair occludes the face.

The segmentation network S takes the target image I_T and the rendered intact face I_R as inputs and produces a binary mask, $M = S(I_T, I_R)$. This mask predicts whether a pixel in the rendered region, Φ , belongs to the face (1) or not (0). Hence, the mask highlighting occlusions can be represented as $1 - M$. We refer to the predicted face region as **valid region**, Ω .

The synergy arises from the two networks operating together. As shown in Fig. 2, the model-based face autoencoder provides the segmentation network with the reconstructed unoccluded face I_R rendered from θ . Through the rendered image the strong appearance prior of the 3DMM is available to the segmentation network. The segmentation network is optimized by comparing I_T and I_R to decide which region should be predicted as occlusions and which not, and can distinguish the regions



Figure 3: In the presence of occlusions, the proposed method can reconstruct faces more faithfully than previous model-based face autoencoders. The images from top to bottom are: target images, results of the MoFA network [27], and the results of ours.

where the face model should adapt to. During the training of the face autoencoder, the occlusion mask, M , predicted by the segmentation network, is used as a pseudo label to exclude the occlusions and ensures that only the unoccluded regions are used to update the encoder and hence the face model can better adapt to the visible part of the face, as shown in the last row in Fig. 3.

3.2 Network Training

Due to the dependencies between the two networks, the EM-like training strategy is needed to enable end-to-end training. The training is split into two steps and updates the two networks alternately. This also enables us to impose different losses on the two sub-networks. In addition, it provides time for each network to adapt before the back-propagation changes the other network, therefore the training process becomes more stable. To enhance the performance further, we propose to take perceptual features into consideration also during the training of segmentation so that the segmentation network can reason based on perceptual information in addition to pixel-wise information. We employ a pretrained ResNet [3], F , and take its extracted intermediate features, $F(I)$, as the perceptual level of an input image I .

Training the segmentation network. When training the segmentation network, the parameters of the face autoencoder are fixed. We assume that the face autoencoder is good enough in estimating the latent variable, θ , to fit the unoccluded face regions. The segmentation is guided by two groups of losses and an additional smoothness term. The losses are listed as follows:

$$L_{img}^{ex} = \left\| \min_{\forall m, n \in N_{i,j}} |I_{T_{i,j \in \Omega}} - I_{R_{m,n}}| \right\|_2^2 \quad (1) \quad L_{img}^{in} = - \left(\sum_{i,j \in \Omega} M_{i,j}^2 \right) / S_{\Phi} \quad (3)$$

$$L_{per}^{ex} = \left\| F(I_{T_{i,j \in \Omega}}) - F(I_{R_{i,j \in \Omega}}) \right\|_2^2 \quad (2) \quad L_{per}^{in} = \left\| F(I_T) - F(I_{R_{i,j \in \Omega}}) \right\|_2^2 \quad (4)$$

The two losses L_{img}^{ex} and L_{per}^{ex} aim at minimizing the distances between the estimated intact face, I_R and the target image I_T . Specifically, L_{img}^{ex} (1) operates at the image level, and L_{per}^{ex} (2) operates at perceptual level, so that the segmentation network predicts also based on semantic features. The image-level neighbour loss, L_{img}^{ex} , compares a pixel, $I_{T_{i,j}}$, on the target image at (i, j) , with the pixels on the rendered image in the corresponding neighbouring region, $N_{i,j}$, so that it is more robust to small misalignments. Since the occluded regions tend to have larger distances to the corresponding ones on the rendered image, including these regions may increase L_{img}^{ex} and L_{per}^{ex} , therefore these regions tend to be discarded by the segmentation network.

The image-level loss, L_{img}^{in} (3) intends to maximize the ratio of the area of the valid region, Ω , to the area, S_{Φ} , of the rendered region, therefore the segmentation network tends to include more pixels in the rendered region. L_{per}^{in} (4) ensures that the semantic face features remain the same as the target after the occlusions are masked out, therefore the unoccluded regions are more likely to be preserved.

Additionally, a regularization term, $L_{bi} = - \sum_{i,j} (M_{i,j} - 0.5)^2$, forces the mask, M , to be binary. The total loss for the segmentation network can be represented as: $L_S = aL_{img}^{ex} + bL_{per}^{ex} + cL_{img}^{in} + dL_{per}^{in} + eL_{bi}$, where $a = 15$, $b = 3$, $c = 0.5$, and $d = 2.5$, and $e = 10$. During training, the network finds a balance point between discarding pixels and preserving pixels by reaching an overall decrease in the total loss.

The **face autoencoder** is optimized to better fit the unoccluded face regions, with assumption that the segmentation network, S , can predict the valid region Ω well enough. The losses for training the encoder include:

$$L_{img}^R = \left\| I_{T_{i,j} \in \Omega} - I_{R_{i,j} \in \Omega} \right\|_2^2 \quad (5) \quad L_{per}^R = \left\| F(I_T) - F(I_R) \right\|_2^2 \quad (6) \quad L_{lm} = \left\| lm_T - lm_R \right\|_2^2 \quad (7)$$

The training of face autoencoder is guided by two reconstruction losses: L_{img}^R (5) at image level and L_{per}^R (6) at perceptual level. To prevent the face autoencoder from taking the shortcut and not fitting to any pixels so that the reconstruction losses become zero, L_{img}^{in} (3) is also implemented during its training. In addition, the landmark loss (7) is used to estimate the pose, where lm_T and lm_R stand for the landmark coordinates on I_T and I_R , respectively. We set the weights for the landmarks on the eyebrows as 0.1, the ones on the contour as 0.2, and the rest as 1. A regularization term is also required for the 3DMM: $L_{reg} = \left\| \theta \right\|_2^2$. To sum up, the loss for training the face autoencoder can be represented as: $L_R = fL_{img}^R + gL_{per}^R + hL_{img}^{in} + iL_{lm} + jL_{reg}$, where $f = 4$, $g = 0.5$, $h = 0.5$, $i = 0.01$, and $j = 0.067$.

3.3 Unsupervised Network Initialization

Our EM-like training strategy needs to be initialized. Before combining the sub-networks together, it is expected that the models do not fit any occlusions, even if some small face regions are not reconstructed well. Therefore, an occlusion robust function is proposed to generate preliminary masks for unsupervised initialization.

$$\log(P_{face_{i,j}}) = -\frac{1}{2\sigma^2}(I_{T_{i,j}} - I_{R_{i,j}})^2 + N_c \quad (8) \quad M_{pre_{i,j}} = \begin{cases} 1 & \text{if } (I_{T_{i,j}} - I_{R_{i,j}})^2 < \xi \\ 0 & \text{otherwise} \end{cases} \quad (9)$$

We assume that the reconstruction error at pixel (i, j) in the face regions follows a 0-mean Gaussian Distribution. Therefore we can express the log-likelihood that a pixel belongs to the face regions as $\log(P_{face})$ (8), where σ and N_c are constant. We also assume that the values of the non-face pixels follow a uniform distribution, so $\log(P_{non-face})$ is a constant. Then we can decide whether a pixel should be classified as face or not by comparing the log-likelihoods, as shown in equation (9). Empirically, ξ is set to 0.17. The face autoencoder is pre-trained with this occlusion robust function to prevent it from fitting to occlusions, and then the segmentation network is pre-trained in a supervised way by taking the preliminary masks as pseudo mask labels for M .

4 Experiments

In the following section, we conduct systematic experiments, and the results show that our weakly-supervised method reaches the state-of-the-art occlusion segmentation results and competitive 3D face reconstruction compared to the state-of-the-art and the methods that use full supervision in terms of occlusion labels. Our ablation study demonstrates the effectiveness of the segmentation network and our proposed training losses.

4.1 Experiment setting

Our reconstruction network uses the Basel Face Model (BFM) 2017 [12] as the 3D face morphable model, with the differentiable renderer proposed in [14]. The segmentation network follows the UNet architecture [23]. The proposed pipeline is trained on the CelebA-HQ trainset [17], following their protocol. All images are rigidly aligned based on their face landmarks as described in [17]. The perceptual features are extracted by a pre-trained VGG2 [3]. To train the face autoencoder, landmarks in the center of the face are detected using Dlib [13], and the ones on the contour are detected using the method of [2]. During training, the Adadelta optimizer is used, with an initial learning rate of 0.06, and a decay rate of 0.99 at every 5k iterations. The learning rate for the segmentation network is 0.06 times the one for the reconstruction network. In every 30k iterations, 25k iters are for the face autoencoder training, and the rest are for training the segmentation network. For initialization, the face autoencoder is trained for 300k iterations, with batch size 12. Afterwards, the face autoencoder and segmentation network are trained jointly for 400k iterations, with a batch size of 6. The speed is evaluated on a NVIDIA RTX 2080 Ti, with batch size 6. It takes about 120 hours to train the initialized face autoencoder, and about 98 hours to train the complete pipeline. After the training, it takes less than one second to perform a 3D face reconstruction and occlusion segmentation.

Baselines. We compare our method with two state-of-the-art model-based face autoencoders, i.e. the MoFA [27] and the Deep3D [5]. Additionally, to achieve fair comparison between our proposed weakly-supervised method and supervised methods, we train the MoFA network in supervised settings with the perceptual loss L_{per}^R to provide baselines for fair comparison, since the standard MoFA network does not handle occlusions explicitly. More specifically, the supervised pipelines use the ground truth (GT) masks provided by the CelebA-HQ database to exclude occlusions during training. Two data augmentation methods for occlusion handling, i.e. the cutmix

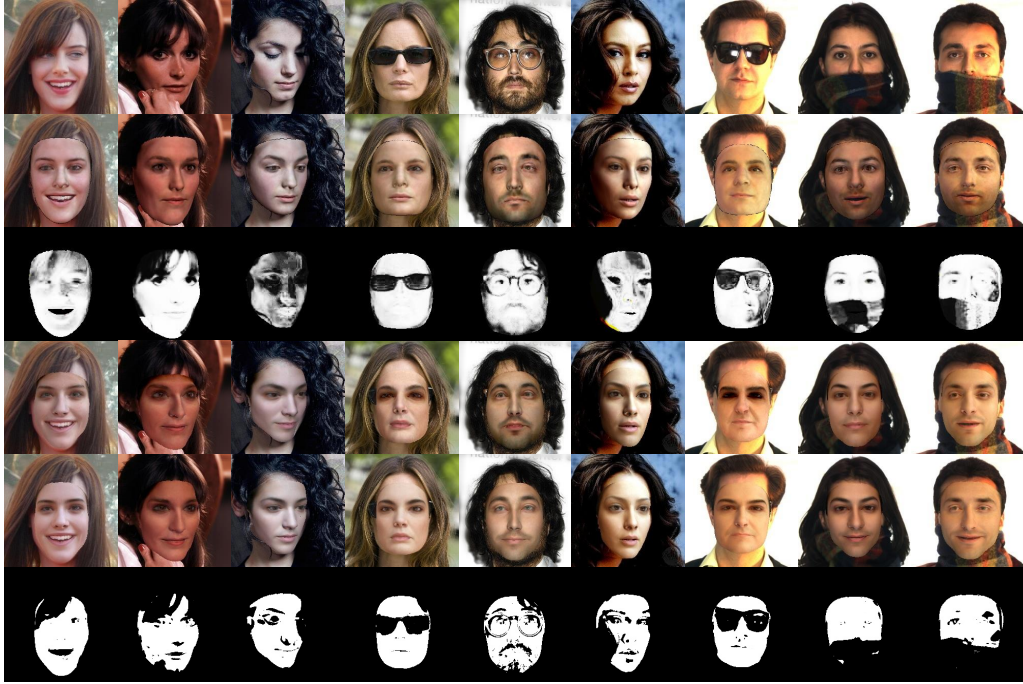


Figure 4: Qualitative comparison on reconstruction and segmentation results between the Deep3D [5] network (the 2nd and 3rd rows), the MoFA network [27] (the 4th row), and the proposed method (the last two rows) on occluded faces from the CelebA-HQ testset (the first 6 columns) and the AR database (the last 3 columns).

[32] and cutout [6], are also implemented to enhance the performance of the supervised pipelines. We refer to the three baselines as Supervised MoFA, MoFA cutmix, and MoFA cutout, respectively.

The CelebA-HQ testset [17] and the AR database [19] are used for evaluating the effectiveness of segmentation. The former provides manually labeled masks for skin, hair, accessories, and so on, and we merge all the masks to obtain the GT masks. For the AR database, 120 manually-segmented results in [7] are used as GT masks. In the following, we provide both qualitative and quantitative results. The standard deviation is provided after \pm . The CelebA-HQ database and the AR database are publicly available and our access to the occlusion labels for the AR dataset is authorized by the authors of [7]. The data used in our paper does not contain harmful information or invade personal information.

4.2 Qualitative Results

Fig. 7 shows some results of the Deep3D network, the MoFA network, and our proposed method for qualitative comparison. The segmentation masks provided by the Deep3D result from a skin detector which assumes that skin color follows the simple multivariate Gaussian distribution. It shows that in our segmentation results, some skin-colored occlusions are better detected, and some small occlusions are also located well. Furthermore, our segmentation is more robust to illumination variations. It can also be observed from the reconstructed images that the illumination and texture of the faces are better estimated. Visually speaking, our method reaches competitive fitting results and improved segmentation masks. Please refer to the supplementary materials for more quantitative results.

4.3 Reconstruction Quality

To quantify the fitting accuracy and how much the fitting result gets misled by occlusions, we compute the Root Mean Square Error (RMSE) between the input image and the reconstructed image inside visible face regions, with provided GT segmentation masks. We compare different methods on the CelebA-HQ testset (referred to as 'CelebA-Overall'), and two randomly-selected occluded (750 random images) and unoccluded subsets (558 random images), which are referred to as 'CelebA-Occluded' and 'CelebA-Unoccluded', respectively. As shown in Tab. 1, our fitting accuracy is competitive to the fully supervised MoFA with data augmentation (i.e. the cutout and cutmix), and the Deep3D.

Table 1: RMSE on the CelebA-HQ testsets and the AR testset.

Testset	MoFA [27]	Supervised MoFA	MoFA cutmix	MoFA cutout	Deep3D [5]	Proposed
CelebA-Unoccluded	8.01 ± 0.47	7.98 ± 0.44	7.95 ± 0.44	8.00 ± 0.44	8.27 ± 0.39	7.68 ± 0.47
CelebA-Occluded	8.54 ± 0.53	8.44 ± 0.52	8.45 ± 0.52	8.45 ± 0.51	8.60 ± 0.54	8.10 ± 0.54
CelebA-Overall	8.31 ± 0.55	8.25 ± 0.52	8.23 ± 0.52	8.26 ± 0.51	8.46 ± 0.47	7.91 ± 0.54
AR-overall	8.13 ± 0.48	8.39 ± 0.56	8.32 ± 0.54	8.31 ± 0.50	8.59 ± 0.51	8.20 ± 0.52

4.4 Occlusion Segmentation

The accuracy of occlusion segmentation is indicated by four indices: accuracy (ACC), precision (Positive Predictive Value, PPV), recall rate (True Positive Rate, TPR), and F1 score (F1). These indices are only calculated inside the rendered regions for both MoFA-based methods and the Deep3D. We also compare our method with the work of [7] on the AR database. Tab. 2 shows the experimental results on the CelebA-HQ testset, and Tab. 3 shows the results on the AR database. We separate the AR dataset into three subsets, which include faces without occlusions (neutral), faces with glasses (glasses), and faces with scarves (scarf). According to Tab. 2 and Tab. 3, the masks predicted by our method show a higher accuracy, recall rate, and F1 score, and competitive precision compared to the skin detector used in [5] and the segmentation method proposed in [7].

Table 2: Evaluation of occlusion segmentation accuracy on the CelebA-HQ testsets.

Method	CelebA-Unoccluded				CelebA-Occluded				CelebA-Overall			
	ACC	PPV	TPR	F1	ACC	PPV	TPR	F1	ACC	PPV	TPR	F1
Deep3D [5]	0.90	0.97	0.93	0.94 ± 0.06	0.80	0.84	0.92	0.87 ± 0.07	0.90	0.91	0.93	0.91 ± 0.07
Proposed	0.94	0.98	0.96	0.97 ± 0.02	0.88	0.92	0.93	0.92 ± 0.06	0.91	0.95	0.95	0.95 ± 0.04

Table 3: Evaluation of occlusion segmentation accuracy on the AR testsets.

Method	neutral				glasses				scarf			
	ACC	PPV	TPR	F1	ACC	PPV	TPR	F1	ACC	PPV	TPR	F1
Deep3D [5]	0.83	0.90	0.91	0.90 ± 0.04	0.81	0.82	0.90	0.86 ± 0.06	0.76	0.76	0.90	0.82 ± 0.06
Egger et al. [7]	-	-	-	0.90	-	-	-	0.87	-	-	-	0.86
Proposed	0.94	0.92	0.99	0.96 ± 0.03	0.88	0.92	0.89	0.90 ± 0.04	0.88	0.93	0.89	0.90 ± 0.06

4.5 Ablation Study

In this section, we verify the usefulness of the segmentation network and the losses for its training. We compare the performances of ablated pipelines on the AR testset, since the samples are with heavier occlusions. The pre-trained model using the occlusion robust function is referred to as 'Pretrained'. We refer to the segmentation network trained with the pixel-wise reconstruction loss L_{img}^R instead of the neighbouring loss L_{img}^{ex} as 'Baseline', and no other losses are used. The 'Neighbour' pipeline refers to the segmentation network where we substitute the neighbouring loss L_{img}^{ex} for the pixel-wise loss in the 'Baseline', and the 'Perceptual' pipeline stands for baseline with two perceptual losses, L_{per}^{ex} and L_{per}^{in} .

The results in Tab. 4 indicates that with the segmentation network, no matter what type of losses are used, the segmentation results excel the pretrained model in almost all the indices, except for the precision, which verifies the usefulness of the segmentation network. In addition, it is also observed that when there are no occlusions, the gap among the performance of the pipelines with different losses is not very obvious, while the gap becomes larger under occlusions (i.e. glasses and scarves). Comparison between the 'Proposed' pipeline and the 'Neighbour' pipeline shows that the perceptual losses, L_{per}^{ex} and L_{per}^{in} , enhance the accuracy, recall rate, and the F1 score by a large margin. Additionally, the comparison between the 'Perceptual' pipeline and the 'Proposed' pipeline indicates that the image-level neighbouring loss, L_{img}^{ex} , improves most of the indices as well.

Fig. 5 provides the visual comparison among the ablated pipelines. It highlights that the occlusion robust function is not robust to illumination variations, and the segmentation network brings great benefit to the robustness to illumination. The pixel-wise neighbour loss encourages the network to produce smoother results, and the perceptual losses help to locate the occlusions more accurately. Generally, the masks estimated by our proposed method are the best ones.

4.6 Limitations and Societal Impact

The experimental results show that our method can reach competitive fitting accuracy, and can provide reliable occlusion masks in a weakly-supervised way. Despite this, there are several limitations.

Table 4: Ablation study on the AR testsets.

Method	neutral				glasses				scarf			
	ACC	PPV	TPR	F1	ACC	PPV	TPR	F1	ACC	PPV	TPR	F1
Pretrained	0.92	0.96	0.92	0.94 ± 0.05	0.70	0.92	0.59	0.71 ± 0.12	0.70	0.95	0.56	0.70 ± 0.12
Baseline	0.94	0.94	0.97	0.95 ± 0.03	0.80	0.92	0.78	0.84 ± 0.06	0.81	0.94	0.75	0.83 ± 0.07
Neighbour	0.93	0.93	0.98	0.95 ± 0.03	0.83	0.93	0.81	0.86 ± 0.06	0.83	0.92	0.80	0.85 ± 0.08
Perceptual	0.94	0.94	0.98	0.96 ± 0.03	0.85	0.91	0.86	0.88 ± 0.04	0.85	0.93	0.84	0.88 ± 0.07
Proposed	0.94	0.92	0.99	0.96 ± 0.03	0.88	0.92	0.89	0.90 ± 0.04	0.88	0.93	0.89	0.90 ± 0.06

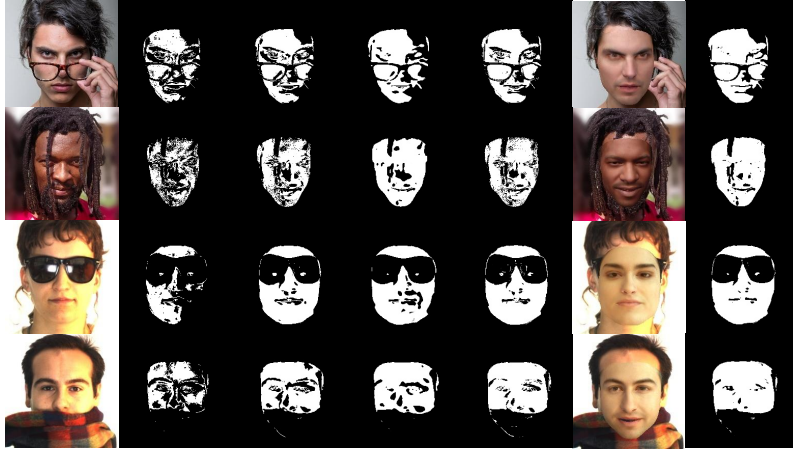


Figure 5: Qualitative comparison for ablation study. From left to right: target images, masks estimated by the 'Pretrained', 'Baseline', 'Neighbour', and 'Perceptual' pipelines, and the reconstruction results and predicted masks of the proposed pipelines, respectively.

The main issue is that the segmentation performance relies largely on the generative ability of the face model. If the models are too expressive, and can even fit the occlusions, then the segmentation network will not expel the occlusions properly. On the other hand, if the models under-fit the target images, the segmentation network tends to regard more pixels as occlusions. The two problems can both be observed in the eye region: When there are sunglasses, the model may consider part of it as eyebrow, which will then be taken as face regions by the segmentation network. When the eyes cannot be properly reconstructed, some pixels will be regarded as occlusions. Although the latter problem is solved partially by the neighbouring loss, which enhances the robustness to small mis-alignments, there is still space for improvement. Additionally, we only predict occlusions inside the rendered face region and do not take the remaining part into consideration. We assume that using a full-face model or a head model can solve this problem.

As for the societal impact, in general, our proposed pipeline has the potential to bring face reconstruction to the real world and to save costs of occlusion labeling, which is generally required in many existing deep-learning-based methods. The model-based reconstruction methods improved by our method could contribute to many applications, including Augmented Reality (AR), Virtual Reality (VR), surveillance, 3D design, and so on. Each of these applications may bring societal and economic benefits, and risks at the same time: The application of AR or VR could bring profits to the entertainment industry and also may result in unethical practices such as demonizing the image of others, identity fraud, and so on. The application of surveillance could help arrest criminals, yet might also invade the privacy and safety of others. The application in 3D design enables quick capture of the 3D shape of an existing face but might also cause problems in portrait rights.

To mitigate the risks, we would encourage researchers and developers in related areas to think about the following questions before bringing this technique to the real world: How to distinguish the distorted personal information, and the machine-generated data from authentic data? How to prevent malicious users from accessing personal data and how to be aware that the data has been accessed? If the generated results are too realistic, what actions could policymakers take to protect normal people from being deceived?

5 Conclusion

In this paper, we have shown how to solve face reconstruction and occlusion robustness jointly in a weakly-supervised way, so as to enhance the robustness to occlusions for model-based face autoencoders in unconstrained environments. Comprehensive experiments have shown that our method not only reaches state-of-the-art fitting

accuracy, but also can provide better segmentation masks. We believe that the fundamental concepts of our approach can go beyond the context of face reconstruction and will inspire future work. More specifically, we expect that our pipeline will be extended to many other implementations, such as human body reconstruction, or object reconstruction. We also expect that the masks will be useful for other tasks, e.g. image completion, recognition, or more.

Acknowledgement Chunlu Li is funded by the China Scholarship Council (CSC) from the Ministry of Education of P.R. China. B.Egger is supported by a PostDoc Mobility Grant, Swiss National Science Foundation P400P2_191110. The authors would like to express their sincere gratitude to the sponsors, as well as Tatsuro Koizumi and William A. P. Smith who offered the MoFA re-implementation.

References

- [1] V. Blanz and T. Vetter. Face recognition based on fitting a 3d morphable model. *IEEE Transactions on pattern analysis and machine intelligence*, 25(9):1063–1074, 2003.
- [2] A. Bulat and G. Tzimiropoulos. How far are we from solving the 2d & 3d face alignment problem? (and a dataset of 230,000 3d facial landmarks). In *International Conference on Computer Vision*, 2017.
- [3] Q. Cao, L. Shen, W. Xie, O. M. Parkhi, and A. Zisserman. Vggface2: A dataset for recognising faces across pose and age. In *2018 13th IEEE international conference on automatic face & gesture recognition (FG 2018)*, pages 67–74. IEEE, 2018.
- [4] M. De Smet, R. Fransens, and L. Van Gool. A generalized em approach for 3d model based face recognition under occlusions. In *2006 IEEE Computer Society Conference on Computer Vision and Pattern Recognition (CVPR’06)*, volume 2, pages 1423–1430, 2006.
- [5] Y. Deng, J. Yang, S. Xu, D. Chen, Y. Jia, and X. Tong. Accurate 3d face reconstruction with weakly-supervised learning: From single image to image set. In *Proceedings of the IEEE/CVF Conference on Computer Vision and Pattern Recognition Workshops*, pages 0–0, 2019.
- [6] T. DeVries and G. W. Taylor. Improved regularization of convolutional neural networks with cutout. *arXiv preprint arXiv:1708.04552*, 2017.
- [7] B. Egger, S. Schönborn, A. Schneider, A. Kortylewski, A. Morel-Forster, C. Blumer, and T. Vetter. Occlusion-aware 3d morphable models and an illumination prior for face image analysis. *International Journal of Computer Vision*, 126(12):1269–1287, 2018.
- [8] B. Egger, W. A. Smith, A. Tewari, S. Wuhrer, M. Zollhoefer, T. Beeler, F. Bernard, T. Bolkart, A. Kortylewski, S. Romdhani, et al. 3d morphable face models—past, present, and future. *ACM Transactions on Graphics (TOG)*, 39(5):1–38, 2020.
- [9] Y. Feng, H. Feng, M. J. Black, and T. Bolkart. Learning an animatable detailed 3d face model from in-the-wild images. *arXiv preprint arXiv:2012.04012*, 2020.
- [10] B. Gecer, S. Ploumpis, I. Kotsia, and S. Zafeiriou. Ganfit: Generative adversarial network fitting for high fidelity 3d face reconstruction. In *Proceedings of the IEEE/CVF Conference on Computer Vision and Pattern Recognition (CVPR)*, June 2019.
- [11] K. Genova, F. Cole, A. Maschinot, A. Sarna, D. Vlasic, and W. T. Freeman. Unsupervised training for 3d morphable model regression. In *Proceedings of the IEEE Conference on Computer Vision and Pattern Recognition*, pages 8377–8386, 2018.
- [12] T. Gerig, A. Morel-Forster, C. Blumer, B. Egger, M. Luthi, S. Schönborn, and T. Vetter. Morphable face models—an open framework. In *2018 13th IEEE International Conference on Automatic Face & Gesture Recognition (FG 2018)*, pages 75–82. IEEE, 2018.
- [13] D. E. King. Dlib-ml: A machine learning toolkit. *Journal of Machine Learning Research*, 10:1755–1758, 2009.
- [14] T. Koizumi and W. A. Smith. “look ma, no landmarks!”—unsupervised, model-based dense face alignment. In *European Conference on Computer Vision*, pages 690–706. Springer, 2020.
- [15] A. Kortylewski, A. Schneider, T. Gerig, B. Egger, A. Morel-Forster, and T. Vetter. Training deep face recognition systems with synthetic data. *arXiv preprint arXiv:1802.05891*, 2018.
- [16] A. Kortylewski, M. Wieser, A. Morel-Forster, A. Wicczorek, S. Parbhoo, V. Roth, and T. Vetter. Informed mcmc with bayesian neural networks for facial image analysis. *arXiv preprint arXiv:1811.07969*, 2018.
- [17] Z. Liu, P. Luo, X. Wang, and X. Tang. Deep learning face attributes in the wild. In *Proceedings of International Conference on Computer Vision (ICCV)*, December 2015.
- [18] F. Maninchedda, C. Häne, B. Jaquet, A. Delaunoy, and M. Pollefeys. Semantic 3d reconstruction of heads. In *European conference on computer vision*, pages 667–683. Springer, 2016.
- [19] A. Martinez and R. Benavente. The ar face database. *Tech. Rep. 24 CVC Technical Report*, 01 1998.

- [20] A. Morel-Forster. *Generative shape and image analysis by combining Gaussian processes and MCMC sampling*. PhD thesis, University_of_Basel, 2016.
- [21] E. Richardson, M. Sela, R. Or-El, and R. Kimmel. Learning detailed face reconstruction from a single image. In *Proceedings of the IEEE Conference on Computer Vision and Pattern Recognition (CVPR)*, July 2017.
- [22] S. Romdhani and T. Vetter. Efficient, robust and accurate fitting of a 3d morphable model. In *ICCV*, volume 3, pages 59–66, 2003.
- [23] O. Ronneberger, P. Fischer, and T. Brox. U-net: Convolutional networks for biomedical image segmentation. In *International Conference on Medical image computing and computer-assisted intervention*, pages 234–241. Springer, 2015.
- [24] Z. Ruan, C. Zou, L. Wu, G. Wu, and L. Wang. Sadrnet: Self-aligned dual face regression networks for robust 3d dense face alignment and reconstruction. *arXiv preprint arXiv:2106.03021*, 2021.
- [25] S. Saito, T. Li, and H. Li. Real-time facial segmentation and performance capture from rgb input. In *European conference on computer vision*, pages 244–261. Springer, 2016.
- [26] S. Sanyal, T. Bolkart, H. Feng, and M. J. Black. Learning to regress 3d face shape and expression from an image without 3d supervision. In *Proceedings of the IEEE/CVF Conference on Computer Vision and Pattern Recognition*, pages 7763–7772, 2019.
- [27] A. Tewari, M. Zollhofer, H. Kim, P. Garrido, F. Bernard, P. Perez, and C. Theobalt. Mofa: Model-based deep convolutional face autoencoder for unsupervised monocular reconstruction. In *Proceedings of the IEEE International Conference on Computer Vision Workshops*, pages 1274–1283, 2017.
- [28] A. Tewari, M. Zollhofer, P. Garrido, F. Bernard, H. Kim, P. Pérez, and C. Theobalt. Self-supervised multi-level face model learning for monocular reconstruction at over 250 hz. In *Proceedings of the IEEE Conference on Computer Vision and Pattern Recognition (CVPR)*, June 2018.
- [29] A. T. Tran, T. Hassner, I. Masi, E. Paz, Y. Nirkin, and G. Medioni. Extreme 3d face reconstruction: Seeing through occlusions. In *2018 IEEE/CVF Conference on Computer Vision and Pattern Recognition*, pages 3935–3944, 2018.
- [30] L. Tran, F. Liu, and X. Liu. Towards high-fidelity nonlinear 3d face morphable model. In *Proceedings of the IEEE/CVF Conference on Computer Vision and Pattern Recognition*, pages 1126–1135, 2019.
- [31] I. Yildirim, M. Janner, M. Belledonne, C. Wallraven, W. Freiwald, and J. Tenenbaum. Causal and compositional generative models in online perception. In *CogSci*, 2017.
- [32] S. Yun, D. Han, S. J. Oh, S. Chun, J. Choe, and Y. Yoo. Cutmix: Regularization strategy to train strong classifiers with localizable features. In *Proceedings of the IEEE/CVF International Conference on Computer Vision*, pages 6023–6032, 2019.
- [33] X. Zhu, J. Yan, D. Yi, Z. Lei, and S. Z. Li. Discriminative 3d morphable model fitting. In *2015 11th IEEE International Conference and Workshops on Automatic Face and Gesture Recognition (FG)*, volume 1, pages 1–8. IEEE, 2015.

A Appendix: Qualitative Comparison

A.1 Face Reconstruction and Occlusion Segmentation



Figure 6: Comparison on **random samples** in the Celeb A HQ [17] and the AR [19] testsets. (a) Target image. (b) and (c) Reconstruction and segmentation results of the Deep3D network [5]. (d) Reconstructed result of the MoFA network [27]. (e) and (f) Reconstruction and segmentation results of ours.



Figure 7: Comparison on samples with **extreme illumination** conditions in the Celeb A HQ [17] and the AR [19] testsets. (a) Target image. (b) and (c) Reconstruction and segmentation results of the Deep3D network [5]. (d) Reconstructed result of the MoFA network [27]. (e) and (f) Reconstruction and segmentation results of ours.



Figure 8: Comparison on samples with occlusions that the **skin detector in [5] fails** to locate in the Celeb A HQ testset [17]. (a) Target image. (b) and (c) Reconstruction and segmentation results of the Deep3D network [5]. (d) Reconstructed result of the MoFA network [27]. (e) and (f) Reconstruction and segmentation results of ours.

A.2 Ablation Study



Figure 9: Qualitative comparison for ablation study on the Celeb A HQ testset [17]. From left to right are (a) target images, masks estimated by the (b) 'Pretrained', (c) 'Baseline', (d) 'Neighbour', and (e) 'Perceptual' pipelines, and (f) the reconstruction results and (g) predicted masks of the proposed pipelines, respectively.

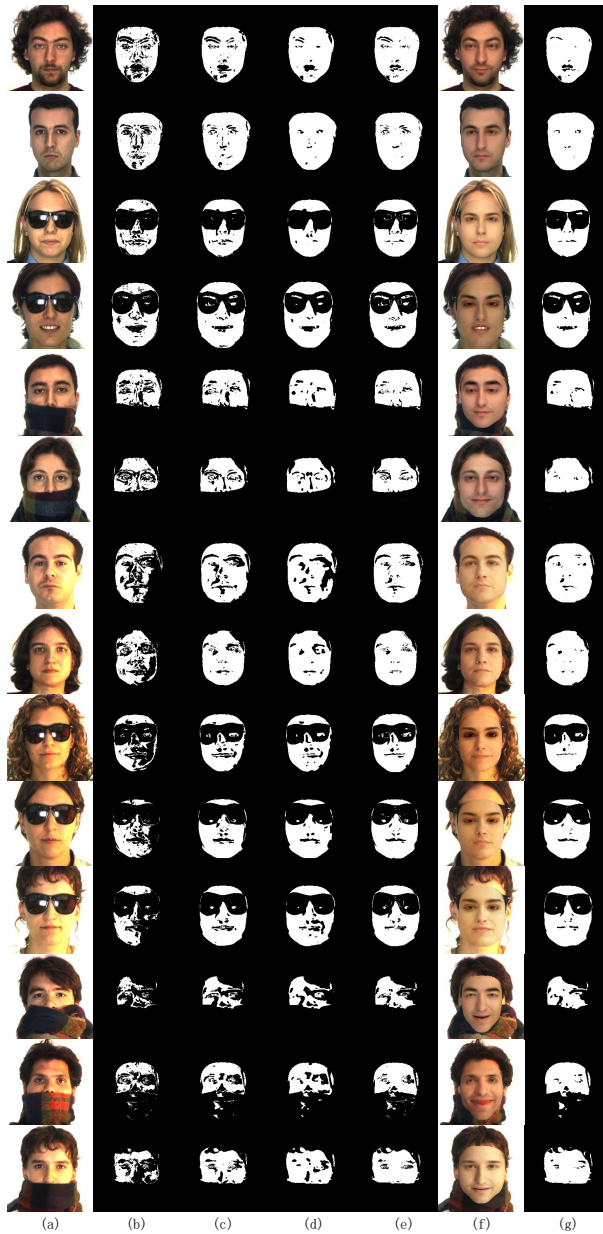


Figure 10: Qualitative comparison for ablation study on the AR testset [19]. From left to right are (a) target images, masks estimated by the (b) 'Pretrained', (c) 'Baseline', (d) 'Neighbour', and (e) 'Perceptual' pipelines, and (f) the reconstruction results and (g) predicted masks of the proposed pipelines, respectively.